Frozen-Core versus Fully-Correlated Configuration Interaction on the Ground and Lowest Excited States of N^+ and N

A.Y. Hussein* and N.H. Ali

Department of Physics, College of Education, Mustansiriyah University, Baghdad, Iraq

Received: 22.11.2022 & Accepted: 13.02.2023

Doi: 10.12693/APhysPolA.143.316 *e-mail: adnanyousif@uomustansiriyah.edu.iq

We present nonrelativistic frozen-core and fully-correlated configuration interaction calculations for the ground and lowest excited terms of $N^+(^3P$ and $^1D)$ and $N(^4S^o$ and $^2D^o)$ belonging to the $2s^2 2p^n$ configuration with $n = 2$ and $n = 3$ for N^+ and N, respectively. Both the *a priori* selected configuration interaction with truncation energy error and configuration interaction by parts techniques are employed to manage the wave function expansion and to handle the configuration interaction eigenvalue problem, respectively. Systematic comparisons between the frozen-core and fully-correlated configuration interaction energies and the corresponding excitation energies and the related ionization potential convergence with respect to the configuration interaction excitation level are reported. Comparison of our results for the total nonrelativistic energies, excitation energies, and ionization potential displays good improvement over previous theoretical results and very good agreement with the experiment.

topics: configuration interaction, nitrogen, excitation energy, ionization potential

1. Introduction

Recently, one of us [1] has calculated excitation energies, ionization potential, and binding energies related to the ground state and the two lowest excited states belonging to P^+, P, and P^-, using nonrelativistic and relativistic configuration interaction (CI) method. From both chemical and physical points of view, both N and P have the same ns^2np^3 valence shell electron configuration and, consequently, the same term multiplet. On the other hand, emission lines of N-like ions are highly beneficial for diagnosing the temperature, density, and composition of solar, astrophysical, and fusion plasmas [2]. In order to interpret their line intensity ratios, an accurate atomic parameter such as energy levels, ionization potentials, transition probabilities, and collision strengths is required. Calculation of the heat of various reactions and physical changes requires the determination of the ionization potential, which is an important issue for both theoretical and experimental interests. In this work, the nonrelativistic CI method has been utilized to report that both the ground ^3P term and the lowest excited ^1D term belong to the $2s^2 2p^2$ configuration of N^+, and both the ground $^4S^o$ term and the lowest excited $^2D^o$ term belong to the $2s^2 2p^3$ configuration of N. In Sect. 2, we review the main features of the nonrelativistic CI theory. In Sect. 3, we give an outline of the frozen-core approximation employed to reduce the large CI expansion. Section 4 deals with the construction of atomic orbitals in terms of a primitive function set, while Sect. 5 displays and discusses the present results. Finally, the conclusions are presented in Sect. 6.

2. Outline of CI theory

In the nonrelativistic CI method, an atomic bound state labeled μ and carrying total orbital angular momentum L and total spin S, as well as a given parity, can be described by the wave function Ψ_μ expressed as [3–5]

$$\Psi_\mu = \sum_{K=1}^{K_x} \sum_{g=1}^{g_K} F_{gK}\, C_{gK}, \tag{1}$$

where F_{gK} is the many-electron basis functions referred to as configuration state functions (CSFs). Now F_{gK} can be expressed as a successively orthogonalized linear combination of n_K Slater determinants D_{iK}, obtained upon applying the symmetric projection operator $O(\Gamma, \gamma)$ [6]. Therefore,

$$F_{gK} = O(\Gamma, \gamma) \sum_{i=1}^{g} D_{iK}\, b_i^g = \sum_{i=1}^{n_K} D_{iK}\, c_i^g, \tag{2}$$

where Γ is the pertinent symmetry for either L^2 or S^2 operators for a given irreducible representation γ. The indexes K and g are labels of configuration and degenerate element, respectively. The set of all excited F_{gK} formed by the set of all ordered configurations differing just in the labels of the correlation orbitals of each irreducible representation is

called a subclass, while the set of subclasses that remain invariant upon nonsingular transformations of the correlation orbitals is called a class [7]. Within a subclass, the b_i^g and c_i^g coefficients in (2) are the same — in magnitude and sign.

The matrix representation of Schrödinger's equation obtained upon variation of the total energy with respect to expansion coefficients $\boldsymbol{C}_\mu$ is

$$H\boldsymbol{C}_\mu = E_\mu^{\mathrm{FCI}}\,\boldsymbol{C}_\mu, \tag{3}$$

where H is the representation of the Hamiltonian operator in terms of CSFs or Slater determinants constructed from a given orbital basis set, $\boldsymbol{C}_\mu$ is the variational expansion vector, and E_μ^{FCI} is the full CI (FCI) energy. The nonrelativistic energy E_μ^{nr} (exact eigenvalue of Schrödinger's equation) is related to E_μ^{FCI} through the relation [8]

$$E_\mu^{nr} = E_\mu^{\mathrm{FCI}} + \Delta E_\mu^{\mathrm{OBI}} + \Delta E_\mu^{\mathrm{CI}}, \tag{4}$$

where $\Delta E_\mu^{\mathrm{OBI}}$ is the error due to orbital basis incompleteness (OBI) [9], and $\Delta E_\mu^{\mathrm{CI}}$ represents the error due to any simplification of the frozen-core CI (FCI) computation effected in the evaluation of E_μ^{nr} [10]. Calculation of FCI energy, even with a small system, is computationally difficult due to the huge CI size. Therefore, the FCI space should be reduced in some way to, hopefully, handle the corresponding CI eigenvalue problem. To manage large CI wave function, we use the following procedure. First, *a priori* selected CI (SCI) with truncation energy error [11] takes place to reduce the CI size; however, the resulting CI space may still be too huge for traditional CI and needs to be further truncated into a selected space (S-space). Second, we perform CI by parts (CIBP) [12] in which the S-space is partitioned into several subspaces (S_0, S_1, S_2,..., S_r) of different dimensions (d_0, d_1, d_2,..., d_r), respectively. All CI coefficients in the reference space S_0 are always variational, and all other subspaces S_i, $i = 1, 2, \ldots, r$ will be taken up variationally one after the other. The theoretical basis of *a priori* SCI with truncation energy error and CIBP has been widely discussed elsewhere [11, 12], and we will not go into its details here.

3. Frozen-core approximation

The highly correlated CI method (i.e., CI wave function expansion includes CSFs beyond singles and doubles excitations) suffers from exponentially increasing of CSFs as successively higher excitations from the reference configuration are included, particularly so in cases in which the FCI calculation could be performed. This is the main factor probably hindering comprehensive CI calculations of electronic wavefunctions with large basis sets. In practice, however, it may, hopefully, be more convenient to reduce the number of CSFs in the CI expansion to reduce the computational cost. The CI size reduction can be performed by assuming that the inactive core orbitals are frozen "or fixed." In fact, the advantage of the frozen-core approximation is that it reduces not only the number of CSFs, but also the computational effort required to evaluate the matrix elements associated with the remaining CSFs. In the frozen-core approximation, the lowest-lying atomic orbitals, occupied by the inner-shell electrons, are constrained to remain doubly-occupied in all configurations. A justification for this approximation is that the inner-shell electrons of an atom are less sensitive to their environment than the valence electrons. Nevertheless, the correlation effects involving the electrons in the low-lying core orbitals are neglected. As a result, when transitioning from fully correlated CI (no frozen-core) to frozen-core calculation, core–core and core–valence correlations are no longer considered. Frozen-core CI calculations can be performed practically by allowing only successful CSFs outside He, Ne, Ar,... to generate. The accuracy and efficiency of this approximation are well controlled by a single parameter, i.e., the number of frozen orbitals. In fact, there are two main reasons to employ the frozen-core approximation. The first is that most of the basis sets commonly used in *ab initio* calculations do not provide sufficient flexibility in the core region to accurately describe the correlation of the core electrons [13]. The second reason is motivated by the fact that many experimental observables are related to energy differences, i.e., ionization potential, electron affinity, etc. However, the errors resulting from this approximation are generally comparable to those associated with basis set incompleteness.

4. One-electron basis set

A bound electron's wave function $\phi_{i\ell m m_s}(x)$ can be written as a product of a radial function $R_{i\ell}$, normalized spherical harmonics $Y_{\ell m}(\theta, \varphi)$ [14], and the usual spin function $\delta_{m_s}(\omega)$ describing the state of the electron ($m_s = \pm 12$), i.e.,

$$\phi_{i\ell m m_s}(x) = R_{i\ell}(r)\, Y_{\ell m}(\theta, \varphi)\, \delta_{m_s}(\omega), \tag{5}$$

where x indicates both space (r, θ, φ) and spin (ω) coordinates, respectively. Here $R_{i\ell}$ is chosen to be a linear combination of energy-optimized Slater-type orbitals (STOs) $S_{j\ell}$ [7],

$$R_{i\ell} = \sum_j S_{j\ell}\, a_{j\ell i}, \tag{6}$$

$$S_{j\ell} = \frac{(2\zeta_{j\ell})^{(n_{j\ell}+\frac{1}{2})}}{\sqrt{(2n_{j\ell})!}}\, r^{(n_{j\ell}-1)}\, \exp\left(-\zeta_{j\ell} r\right), \tag{7}$$

where n is the principal quantum number, $a_{j\ell n}$ is the orbital expansion coefficient, and $\zeta_{j\ell}$ is the nonlinear parameter orbital exponent. In our calculation, two types of nonrelativistic CI calculations were performed. The first one is the CI calculation of the valence energy, in which the core-correlation effect is neglected (frozen-core approximation). The second type of CI calculation is the fully-correlated energy, in which all electron correlation contributions within a certain basis set are

TABLE I

Number of STOs per orbital symmetry for $N^+(2s^22p^2)$ ^3P and ^1D states in both frozen-core and fully-correlated calculations at the CISD level of approximation.

Approximation	Term	Basis set composition	No. of STOs
frozen-core	^3P	*10s 9p 6d 5f 5g 4h 4i 3k 2l 2m 1n*	51
	^1D	*10s 9p 7d 6f 5g 5h 4i 3k 3l 2m 2n*	56
fully-correlated	^3P	*9s 8p 6d 4f 2g 1h 1i*	31
	^1D	*9s 8p 6d 5f 2g 2h 1i*	33

TABLE II

Number of STOs per orbital symmetry for $N(2s^22p^3)$ $^4S^o$ and $^2D^o$ states in both frozen-core and fully-correlated calculations at the CISD level of approximation.

Approximation	Term	Basis set composition	No. of STOs
frozen-core	$^4S^o$	*10s 9p 7d 6f 5g 5h 4i 3k 3l 2m 1n*	55
	$^2D^o$	*11s 9p 8d 7f 5g 5h 4i 4k 3l 3m 2n*	61
fully-correlated	$^4S^o$	*8s 8p 6d 5f 2g 2h 1i*	32
	$^2D^o$	*9s 8p 6d 5f 3g 2h 1i*	34

taken into account. In both cases, $N^+(^3P, ^1D)$ and $N(^4S^o, ^2D^o)$, the orbitals $1s$ and $2s$ are initially represented by 7 STOs of the s-type, while the $2p$ orbital is represented by 5 STOs of the p-type. This basis set is composed to satisfy the Hartee–Fock (HF) energy [15] of the considered state. For each irreducible representation (irrep), a new STO is introduced in the form of a set of trial primitives (N_t). Optimization process of N_t trial primitives in the sense of obtaining the lowest energy is at CI limited to single (S) and double (D) excitations (CISD) level of approximation. Thereafter, the orbital space of the wave function is expanded by including all possible CSFs at SD excitations outside the He core, up to the orbital harmonic $\ell = 10$. The STOs basis is automatically optimized until saturation is reached within a prescribed energy threshold decrement (cut-off = 20 μhartree), and one can reach reasonable convergence for a certain type of orbital symmetry. It should be noted that only CSFs interacting with their corresponding reference configuration (HF configuration) are involved during automatic optimization. These "HF interacting spaces" [7] yield the largest contributions to the correlation energy as well as reduce the CPU time for automatic optimization. Likewise, the fully-correlated CI calculations employed the same initial STOs basis as the frozen-core CI calculations except for the fact that automatic optimization was performed on configuration lists including all possible CSFs at SD excitations up to the orbital harmonic $\ell = 6$, within the prescribed energy threshold decrements (cut-off = 400 μhartree). Eventually, the automatic optimization ended with a basis set of energy-optimized STOs, later to be used to compute the corresponding variational upper bound for both valence correlation and fully-correlated CI energies up to triple (T) excitations (CISDT), quadruple (Q) excitations (CISDTQ), quintuple (Qn) excitations (CISDTQQn), sextuple (Se) excitations (CISDTQQnSe) and septuple (Sp) excitations (CISDTQQnSeSp).

In this investigation, we maintain a systematic procedure for the CI calculation in which each excitation level incorporates the same maximum orbital harmonic for each state. Table I presents the number of energy-optimized STOs per each orbital symmetry (column 3), for each term (column 2) of N^+ and for both frozen-core and fully-correlated (column 1) CI calculations. The energy optimization of the ground ^3P term is finished with 51 and 31 STOs for valence correlation and fully-correlated CI calculations, respectively. The excited ^1D term takes relatively higher additional STOs of 56 and 33 for frozen-core and fully-correlated CI calculations, respectively.

Similarly, Table II represents the counterpart of Table I for the ground $^4S^o$ and excited $^2D^o$ terms of N. The energy-optimized STOs for both $^4S^o$ and $^2D^o$ terms proceed in a similar manner to both ^3P and ^1D terms of N^+. However, both $^4S^o$ and $^2D^o$ terms reported more additional STOs per orbital symmetry in each of the frozen-core and fully-correlated approaches with respect to ^3P and ^1D terms of N^+.

5. Results and discussion

In this section, we will report the results of nonrelativistic CI calculations carried out into two schemes: the first is the frozen-core, in which CI expansion includes CSFs generated from outside He core orbitals up to quadruple and quintuple excitation levels for both $N^+(2s^22p^2)$ ^3P, ^1D and $N(2s^22p^3)$ $^4S^o$,$^2D^o$ terms, respectively. The second

TABLE III

Angular momentum-energy convergence for ^3P and ^1D terms of $N^+(2s^22p^2)$. Valence energies E [hartree] and energy-convergence ΔE [μhartree].

ℓ	$E(^3P)$	ΔE	No. of CSFs	$E(^1D)$	ΔE	No. of CSFs
1	−53.93503510467438		634	−53.85521500207359		434
2	−53.98639128024172	−51356.18	1291	−53.91025400035096	−55039.00	1274
3	−53.99273979911247	−6348.51	1781	−53.92189469731616	−11640.69	2168
4	−53.99418343616381	−1443.64	2196	−53.92417626570334	−2281.57	2853
5	−53.99469434932637	−510.91	2490	−53.92496505753687	−788.79	3458
6	−53.99492152773623	−227.18	2760	−53.92530794452659	−342.89	3882
7	−53.99503259019177	−111.07	2934	−53.92547333404052	−165.39	4158
8	−53.99508652347738	−53.93	3027	−53.92556443555691	−91.1	4392
9	−53.99511820422974	−31.68	3100	−53.92561078422519	−46.35	4520
10	−53.99513137119369	−13.17	3127	−53.92563941720704	−28.63	4630

TABLE IV

Angular momentum-energy convergence for ^3P and ^1D terms of $N^+(2s^22p^2)$. Total energies E [hartree] and energy-convergence ΔE [μhartree].

ℓ	$E(^3P)$	ΔE	No. of CSFs	$E(^1D)$	ΔE	No. of CSFs
1	−53.97954587954785		1811	−53.89979705822890		1061
2	−54.03875556762288	−59209.69	3914	−53.96242392874697	−62626.80	2933
3	−54.04633508371431	−7579.52	5200	−53.97537804031013	−12954.12	4943
4	−54.04772902429686	−1393.94	5643	−53.97757913427841	−2201.09	5591
5	−54.04810174993989	−372.72	5775	−53.97830252560567	−723.39	6101
6	−54.04825762428462	−155.88	5855	−53.97852968136614	−227.16	6247

scheme will concern fully-correlated CI calculations in which all possible generated CSFs up to sextuple and septuple excitation levels are taken into account for both $N^+(2s^22p^2)$ ^3P, ^1D and $N(2s^22p^3)$ $^4S^o$, $^2D^o$ terms, respectively.

5.1. The ^3P and ^1D terms of $N^+(2s^22p^2)$

Table III shows the angular momentum-energy pattern of convergence and the corresponding number of CSFs calculated for frozen-core CI calculation of the ground ^3P and excited ^1D terms belonging to $N^+(2s^22p^2)$ at SD excitation level of approximation up to $\ell = 10$.

The ^3P term shows a faster energy convergence pattern with respect to the ^1D term; this result is confirmed in Fig. 1, where the ^3P term displays the lowest number of determinants relative to the ^1D term. At the CISD level, however, the number of CSFs of the ^3P term still exceeds that of the ^1D term for $\ell \leq 2$ at the CISD level.

Similarly, Table IV represents the counterpart of Table III for fully-correlated CI calculation at SD excitation levels up to $\ell = 6$. The ^3P term continues to exhibit faster energy convergence, with a significantly increasing number of CSFs up to $\ell = 6$. Furthermore, a comparison of Tables III and IV

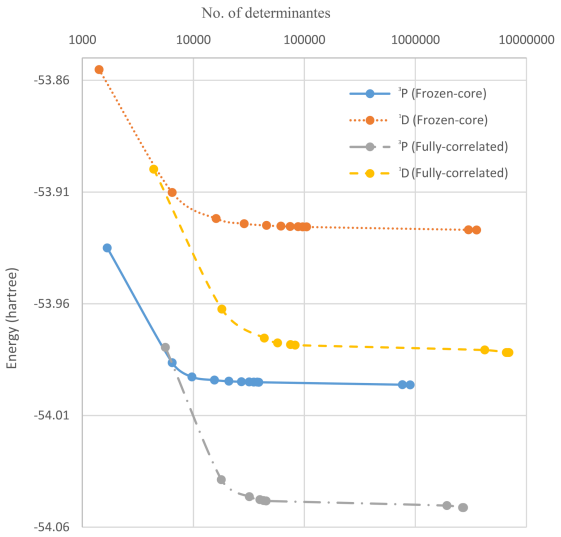

Fig. 1. Energy convergence of the ground ^3P and exited ^1D terms of N^+ with respect to number of determinants (logarithmic scale).

at $\ell = 6$ reveals a shift from frozen-core to fully-correlated CI calculation increased the number of CSFs by approximately 53% and 38% for ^3P and ^1D terms, respectively.

TABLE V

Valence energies (in hartree) and valence correlation energy ΔE [μhartree] of ^3P and ^1D terms of $N^+(2s^22p^2)$, at different CI excitation levels, and the corresponding contributions to excitation energy $EE(^1D–^3P)$ [cm^{-1}] compared with experiment.

Approximation	$E(^3P)$	ΔE	$E(^1D)$	ΔE	$EE(^1D-{}^3P)$
$HF_{(numerical)}$	−53.88800498		−53.80740693		17689.277
HF	−53.8880044114		−53.8074059169		17689.325
CISD	−53.9951313711	107126.960	−53.9256394172	118233.500	15251.721
CISDT	−53.9962289088	1097.538	−53.9269202447	1280.828	15211.493
CISDTQ	−53.9962912298	62.321	−53.9270429547	122.71	15198.240
ΔE^{OBI}	−0.000057756		−0.000093043		-7.745
E^{nr} (this work)	−53.9963489858		−53.9271359977		15190.495
Experiment[a]					15316.2

[a] Ref. [17]

TABLE VI

Total energies (in hartree) and correlation energy ΔE [μhartree] of ^3P and ^1D terms of $N^+(2s^22p^2)$, at different CI excitation levels, and the corresponding contributions to excitation energy $EE(^1D-{}^3P)$ [cm^{-1}] compared with best previous work and experiment.

Approximation	$E(^3P)$	ΔE	$E(^1D)$	ΔE	$EE(^1D-{}^3P)$
$HF_{(numerical)}$	−53.88800498		−53.80740693		17689.277
HF	−53.8880044114		−53.8074059169		17689.325
CISD	−54.0482576243	160253.213	−53.9785296814	171123.765	15303.514
CISDT	-54.0503485226	2090.898	−53.9807302257	2200.544	15279.450
CISDTQ	−54.0512891862	940.664	−53.9818469741	1116.748	15240.804
CISDTQQn	−54.0512900535	0.867	−53.9818484077	1.434	15240.680
CISDTQQnSe	−54.0512900953	0.042	−53.9818485288	0.121	15240.662
ΔE^{OBI}	−0.000168266		−0.000209976		−9.154
E^{nr} (this work)	54.0514583613		−53.9820585048		15231.508
$E^{nr,\,a}$	−54.04674		−53.97732		15235.929
Experiment[b]					15316.2

[a]Ref. [21]; [b]Ref. [17]

Eventually, the values of the angular momentum-energy pattern can be used to deduce the effect of truncation of the virtual correlation space, which can be represented by the orbital basis incomplete error ΔE^{OBI}, obtained as an extrapolation of both the valence and total CISD energy up to $\ell = 400$, as a function of the angular momentum of the energy functional,

$$\Delta E(\ell) = \sum_i \left[E_i(\ell) - E_i^{patt}(\ell)\right]^2, \tag{8}$$

where E_i^{patt} is based on Schwartz's law [16] given by

$$E_i^{patt}(\ell) = a_0(\ell+\delta)^{-4}, \tag{9}$$

where a_0 and δ are adjustable parameters.

The reason for carrying out extrapolation, particularly at the CISD level, comes from the fact that the CISD wave function is dominant, leading to maximum energy correlation contribution among other CI excitation levels. In Table V, we present the valence CI energies at different excitation levels up to SDTQ excitation of approximation for ^3P and ^1D terms of $N^+(2s^22p^2)$ and the corresponding contribution to the excitation energy $EE(^1D–^3P)$. Also, we show the valence correlation energy contributions (columns 3 and 5 for ^3P and ^1D, respectively) for each excitation level, calculated as follows: for CISD, it is equal to the difference between the CISD energy and the HF energy; for CISDT, it is equal to E(CISDT)−E(CISD), and so on. Furthermore, in Table V, we listed two values of HF energies for comparison, calculated in two different approaches. The first approach uses a program developed by C. Froese Fischer [18] based on a solution of the HF equation that uses a numerical basis set. The other approach uses Brown's formula [19],

$$\Delta E_{gK} = (E - H_{gK,gK})\,\frac{C_{gK}^2}{\left(1-C_{gK}^2\right)}. \tag{10}$$

TABLE VII

Angular momentum-energy convergence for $^4S^o$ and $^2D^o$ terms of N($2s^2 2p^3$). Valence energies E [hartree] and energy-convergence ΔE [μhartree].

ℓ	$E(^4S^o)$	ΔE	No. of CSFs	$E(^2D^o)$	ΔE	No. of CSFs
1	−54.44786015516434		453	−54.34643593039574		968
2	−54.51253533805678	−64675.18	866	−54.41632622100514	−69890.29	3332
3	−54.52267134480346	−10136.01	1175	−54.43228850902040	−15962.28	6139
4	−54.52485088131397	−2179.54	1395	−54.43562025739601	−3331.75	8069
5	−54.52560525931290	−754.37	1590	−54.43672916709740	−1108.91	9714
6	−54.52593071712582	−325.46	1732	−54.43720131932312	−472.15	10836
7	−54.52608614094897	−155.43	1819	−54.43743790218403	−236.59	11818
8	−54.52617147169921	−85.33	1891	−54.43756044880467	−122.54	12463
9	−54.52621474427465	−43.27	1932	−54.43763255115464	−72.11	13030
10	−54.52623234033580	−17.6	1946	−54.43767022664217	−37.67	13351

Note that (10) can only be applied after CISD calculation has been completed. The purpose of the comparison between both HF values is to guarantee that our calculated HF energy reaches the HF limit. The agreement of both HF values up to six significant figures confirms the quality of our employed basis. We see that the HF energies account for 99.8% of the nonrelativistic valence CI energies for both ^3P and ^1D terms. On the other hand, the valence correlation energy contribution at the CISD excitation level recovers the majority contribution of the valence correlation energy of 98.9%, 1% for CISDT, and 0.06% for CISDTQ of the ^3P term. This is a consequence of what is called Brillouin's theory [20]. One can expect that doubly excited determinants provide the leading and most important correlation contribution to HF energy. However, one should mention that singles, triples, and quadruples could have contributed to the valence correlation energy through indirect interaction with HF determinants through mixing with the doubly excited determinants. For the excited ^1D term, although the valence correlation energy contribution for different CI excitation levels behaves in the same spirit as the ground ^3P term, there is, however, a little bit of increment on both the CISDT and CISDTQ energy contributions.

Table VI displays the counterpart of Table V for fully-correlated CI calculations, where the total CI energy is illustrated by systematically increasing the excitation level up to SDTQQnSe with the corresponding contribution to the excitation energy.

We can see that the correlation energy contributions for CISDTQQn and CISDTQQnSe clearly converge roughly below 1 μhartree, at least for the ^3P term, whereas it is only a little bit above the 1 μhartree for ^1D term. On the other hand, the convergence of the excitation energy from CISDTQ to CISDTQQnSe stabilized at 15240 cm^{-1}. As a consequence, limiting the maximum excitation level to about a quintuple is usually sufficient to get fairly good accuracy. Our nonrelativistic energy is compared with the best previous nonrelativistic energies [21] for the ^3P and ^1D terms and the corresponding ionization potential, as well as with the experiment [17].

To the best of our knowledge, our upper bound energies for ^3P and ^1D terms of N^+, calculated at CISD, CISDT, CISDTQ, CISDTQQn, and CISDTQQnSe, are the best among available published results.

In both Tables V and VI, we also give ΔE^{OBI}, which we eventually combine with the corresponding CI energy associated with the maximum excitation CI level (full CI energy E^{FCI}) to get the nonrelativistic energies E^{nr} of both frozen-core (Table V) and fully-correlated CI (Table VI) calculations. A comparison of both nonrelativistic valence and total energies in Tables V and VI, respectively, reveals that the fully-correlated CI calculations yield an estimation for excitation energy closer to the experiment than the frozen-core approximation by about 41 cm^{-1}. However, even with taking core-correlation and core–valence contributions [1] into account, the nonrelativistic theory is not always sufficient to achieve better agreement with the experiment. The relativistic effect is expected to be rigorous. According to spectroscopic data [17], the ground ^3P term has three levels that appear, with $J = 0, 1$ and 2, respectively. The corresponding state associated with the excited ^1D term is $J = 2$. Thus, excitation energy should be taken as $EE(^1D - {}^3P) = EE(^1D_2 - {}^3P_0)$.

According to recently published results [1] on phosphorus and two of its ions, both P and P^+ possess an electronic structure similar to N and N^+, respectively. A relativistic correction contribution to the excitation energy $EE(^1D_2 - {}^3P_0)$ of P^+ is reported to be 344 cm^{-1}. However, according to preliminary relativistic calculations, we expect that the relativistic contribution to the $EE(^1D_2 - {}^3P_0)$ of N^+ will not exceed 100 cm^{-1}.

TABLE VIII

Angular momentum-energy convergence for $^4S^o$ and $^2D^o$ terms of N($2s^2 2p^3$). Total energies E [hartree] and energy-convergence ΔE (μhartree].

ℓ	$E(^4S^o)$	ΔE	No. of CSFs	E(^{2}D^o)	ΔE	No. of CSFs
1	−54.49257869126328		1053	−54.39141141736441		2143
2	−54.56586373010639	−73285.04	2028	−54.46939860404672	−77987.19	6223
3	−54.57743846301825	−11574.73	2763	−54.48663363674719	−17235.03	10733
4	−54.57953202089847	−2093.56	2960	−54.49002138638421	−3387.75	13160
5	−54.58022034510598	−688.32	3097	−54.49102318563767	−1001.8	14396
6	−54.58043570767940	−215.36	3136	−54.49132914093828	−305.96	14801

TABLE IX

Valence energies (in hartree) and energy-convergence ΔE [μhartree] of $^4S^o$ and $^2D^o$ terms of N($2s^2 2p^3$), at different CI excitation levels, and the corresponding contributions to excitation energy $EE(^2D^o - {}^4S^o)$ [cm^{-1}] compared with experiment.

Approximation	$E(^4$S$^o)$	ΔE	$E(^2$D$^o)$	ΔE	$EE(^2D^o - {}^4S^o)$
HF$_{\text{(numerical)}}$	−54.40093419		−54.29616933		22993.229
HF	−54.4009341541		−54.2961668390		22993.768
CISD	−54.5262323403	125298.186	−54.4376702267	141503.388	19437.137
CISDT	−54.5292463335	3013.993	−54.4415659898	3895.763	19243.611
CISDTQ	−54.5297735272	527.194	−54.4423357925	769.803	19190.364
CISDTQQn	−54.5297827086	9.1814	−54.4423515685	15.776	19188.917
ΔE^{OBI}	−0.000072963		−0.000086894		−3.058
E^{nr} (this work)	−54.5298556716		−54.4424384625		19185.860
Experiment [b]					19224.464

[a] Ref. [17]

In Fig. 1, we plot the convergence of both the valence and total energies of the ground ^3P and excited ^1D terms of $N^+(2s^2 2p^2)$ as a function of the number of determinants, although the total energy is shifted much lower than that of the corresponding valence energy for both ^3P and ^1D terms. The energy shift between valence and total energy can be interpreted as the core–core and core–valence energy correlation contributions. Furthermore, the sharp drop in CI energies is restricted to the region in which the number of determinants corresponds to SD excitation.

5.2. The $^4S^o$ and $^2D^o$ terms of N($2s^2 2p^3$)

Table VII displays the angular momentum-energy pattern of convergence calculated at the SD excitation level of approximation up to $\ell = 10$ and the corresponding number of CSFs, for the frozen-core CI calculation of the $^4S^o$ and $^2D^o$ terms of N($2s^2 2p^3$). The ground $^4S^o$ term has a faster energy convergence pattern than the excited $^2D^o$ term, with the $^2D^o$ term having 7 times the number of CSFs as the $^4S^o$ term at $\ell = 10$. Similarly, Table VIII represents the counterpart of Table VII for fully-correlated CI calculations up to $\ell = 6$. The $^4S^o$ term still displays faster energy convergence with respect to the $^2D^o$ term. Furthermore, a comparison of Tables VI and VIII at $\ell = 6$ reveals that the number of CSFs increased by about 45% and 37% for $^4S^o$ and $^2D^o$ terms, respectively, upon shifting from frozen-core to fully-correlated CI calculation.

In Table IX, we present the valence CI energies of both $^4S^o$ and $^2D^o$ terms of N and the corresponding contributions to both energy correlation ΔE and the excitation energy $EE(^2D^o - {}^4S^o)$ as a function of CI excitation up to the SDTQQn level. At the HF level of approximation, the calculated $EE(^2D^o - {}^4S^o)$ and one from the experiment have a large discrepancy of 3761 cm^{-1}. As seen in Table IX, more and more energy correlation is gained when going from the SD to the SDTQQ excitation level. However, frozen-core CI calculations still produce $EE(^2D^o - {}^4S^o)$, and that is nearly 39 cm^{-1} less than in the experiment.

When we move to fully-correlated CI calculations shown in Table X, the excitation energy displays almost stable behavior from CISDTQQn to CISDTQQnSeSp. Furthermore, in Table X, we compare our estimated nonrelativistic total energies E^{nr} and the corresponding excitation energy $EE(^2D^o - {}^4S^o)$ with the best previously published results. Our nonrelativistic energies for $^4S^o$ and $^2D^o$ terms represent the best (lowest) upper bounds, and the corresponding $EE(^2D^o - {}^4S^o)$ are in much better agreement than previous results with respect to

TABLE X

Total energies (in hartree) of $^4S^o$ and $^2D^o$ terms of N($2s^2 2p^3$) at different CI excitation levels, and the corresponding contributions to excitation energy [cm^{-1}] compared with best previous calculations and experiment.

Approximation	$E(^4S^o)$	ΔE	$E(^2D^o)$	ΔE	$EE(^2D^o - {}^4S^o)$
$HF_{(numerical)}$	−54.40093419		−54.29616933		22993.229
HF	−54.4009341541		−54.2961668390		22993.768
CISD	−54.5804357077	179501.554	−54.4913291409	195162.302	19556.630
CISDT	−54.5843330374	3897.330	−54.4958414081	4512.267	19421.667
CISDTQ	−54.5856291684	1296.131	−54.4975602023	1718.794	19328.904
CISDTQQn	−54.5856400619	10.894	−54.4975846814	24.4791	19325.922
CISDTQQnSe	−54.5856408586	0.797	−54.4975864837	1.8023	19325.701
CISDTQQnSeSp	−54.5856408669	0.008	−54.4975864884	0.0047	19325.702
ΔE^{OBI}	−0.000259622		−0.000278069		−4.0486
E^{nr} (this work)	−54.5859004889		−54.4978645574		19321.653
E^{nr} [a]	−54.5812				
					21333[b]
E^{nr} [c]	−54.4010		-54.2962		23000.94
Experiment[d]					19224.464

[a]Ref. [22]; [b]Ref. [23]; [c]Ref. [24]; [d] Ref. [17]

TABLE XI

Valence energies (in hartree) of ^3P term of $N^+(2s^2 2p^2)$ and $^4S^o$ term of N($2s^2 2p^3$), at different CI excitation levels, and the corresponding contributions to ionization potential (in meV) compared with experiment.

Approximation	^3P	$^4S^o$	IP($^3P - {}^4S^o$)
$HF_{(numerical)}$	−53.88800498	−54.40093419	13957.521
HF	−53.8880044114	−54.4009341541	13957.536
CISD	−53.9951313711	−54.5262323403	14452.000
CISDT	−53.9962289088	−54.5292463335	14504.150
CISDTQ	−53.9962912298	−54.5297735272	14516.800
CISDTQQn	–	−54.5297827086	14517.049
ΔE^{OBI}	−0.000057756	−0.000072963	0.414
E^{nr} (this work)	−53.9963489858	−54.5298556716	14517.463
Experiment[a]			14534.1

[a]Ref. [25]

the experiment. However, $EE(^2D^o - {}^4S^o)$, corresponding to the estimated nonrelativistic total energies E^{nr} of $^4S^o$ and $^2D^o$, reported an increase in the discrepancy and reached about 97 cm^{-1} above the experiment. To improve the agreement between $EE(^2D^o - {}^4S^o)$ and the experiment, the relativistic effect for both the ground state $^4S^o_{3/2}$ and the excited $^2D^o_{5/2}$ states, viz., $^2D^o_{5/2} - {}^4S^o_{3/2}$ should be included. On the other hand, a comparison between Table IX and Table X of the correlation energy convergence displays the diminishing of ΔE towards 0.008 and 0.0047 μhartree for $^4S^o$ and $^2D^o$ terms, respectively, for fully-correlated CI, which are much below the corresponding frozen-core CISDTQQn.

Figure 2 displays the convergence of both the valence and total energies of the ground $^4S^o$ and excited $^2D^o$ terms of N($2s^2 2p^3$) as a function of the number of determinants. Clearly, both the $^4S^o$ and $^2D^o$ terms exhibit the same characteristic behavior of both ^3P and ^1D terms of N^+ shown in Fig. 1.

5.3. Ionization potential of $^4S^o$

In Tables XI and XII, we combine the energy results of the $N^+(2s^2 2p^2)^3P$ term with the N $(2s^2 2p^3)^4S^o$ term for frozen-core CI calculations (Table XI), and those correspond to fully-correlated CI calculations (Table XII). Furthermore, the ionization potential (IP) contribution is reported for

TABLE XII

Total energies (in hartree) of ^3P term of $N^+(2s^22p^2)$ and $^4S^o$ term of $N(2s^22p^3)$, at different CI excitation levels, and the corresponding contributions to ionization potential (in meV) compared with experiment.

Approximation	^{3}P	$^4S^o$	IP(^{3}P-^{4}S^o)
$HF_{(numerical)}$	−53.88800498	−54.40093419	13957.521
HF	−53.8880044114	−54.4009341541	13957.536
CISD	−54.0482576243	−54.5804357077	14481.310
CISDT	−54.0503485226	−54.5843330374	14530.466
CISDTQ	−54.0512891862	−54.5856291684	14540.138
CISDTQQn	−54.0512900535	−54.5856400619	14540.411
CISDTQQnSe	−54.0512900953	−54.5856408586	14540.432
CISDTQQnSeSp	–	−54.5856408669	14540.432
ΔE^{OBI}	−0.000168266	−0.000259622	2.486
E^{nr} (this work)	−54.0514583613	−54.5859004889	14542.917
			14070[a]
Experiment[b]			14534.1

[a]Ref. [23]; [b]Ref. [25]

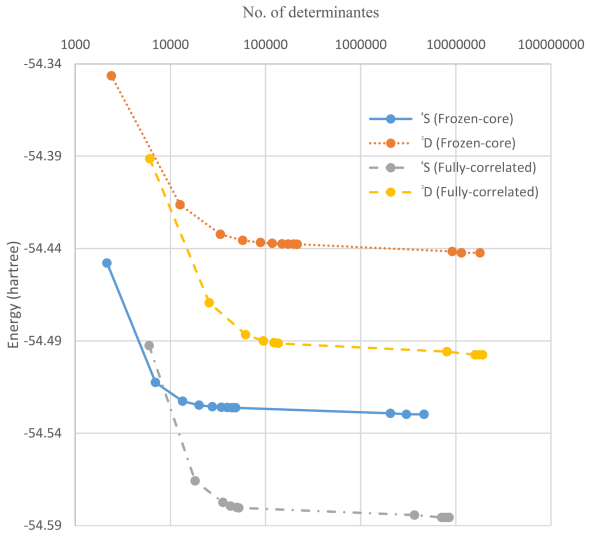

Fig. 2. Energy convergence of the ground $^4S^o$ and exited $^2D^o$ terms of N with respect to number of determinants (logarithmic scale).

different excitation levels. Very good agreement between our calculated ionization potential, estimated at frozen-core approximation (Table XI), and the experiment has been reached, however, there is still a discrepancy of 17 meV. An improvement in the ionization potential upon shifting to fully-correlated CI calculations, in which the discrepancy reduces to only 9 meV with respect to the experiment, was also achieved.

6. Conclusions

We use both frozen-core and fully-correlated approaches in the CI method to calculate the nonrelativistic energy of ^3P and ^1D terms belonging to $N^+(2s^22p^2)$, and $^4S^o$ and $^2D^o$ terms belonging to $N(2s^22p^3)$. Excitation energies $EE(^1D - {}^3P)$ and $EE(^2D^o - {}^4S^o)$ are reported, as well as ionization potential $\mathrm{IP}(^3P - {}^4S^o)$. Furthermore, we give explicit data on the convergence of correlation energy contributions of $EE(^1D - {}^3P)$, $EE(^2D^o - {}^4S^o)$, and $\mathrm{IP}(^3P - {}^4S^o)$ for each excitation level, whether for frozen-core or fully-correlated energies. Also, we compare the results obtained from frozen-core and fully-correlated CI calculations with respect to both previously published results and the experiment. The frozen-core approximation is an effective method to reduce the dimension of the CI eigenvalue problem to be solved and eventually gives results in good agreement with the experiment, however, to reach an excellent agreement with the experiment one still needs to add both core–core and core–valence as well as the relativistic effect. Even with a relatively moderate basis set, fully correlated CI treatment can provide very good agreement with the experiment. We expect, however, that in order to present a real assessment, one needs to add a relativistic effect.

References

[1] A.Y. Hussein, *Phys. Rev. A* **105**, 012809 (2022).

[2] J.J. Mao, J. S. Kaastra, M. Mehdipour, A.J.J. Raassen, L.Y. Gu, J.M. Miller, *Astron. Astrophys.* **607**, A100 (2017).

[3] A.V. Bunge, C.F. Bunge, R. Jáuregui, G. Cisneros, *Comp. Chem.* **13**, 201 (1989).

[4] R. Jáuregui, C. F. Bunge, A. V. Bunge, G. Cisneros, *Comp. Chem.* **13**, 223 (1989).

[5] A.V. Bunge, C.F. Bunge, R. Jáuregui, G. Cisneros, *Comp. Chem.* **13**, 239 (1989).

[6] C.F. Bunge, A.V. Bunge, *Int. J. Quantum Chem.* **7**, 927 (1973).

[7] A.V. Bunge, *J. Chem. Phys.* **53**, 20 (1970).

[8] C.X. Almora-Díaz, H.I. Rivera-Arrieta, C.F. Bunge, *Adv. Quantum Chem.* **72**, 129 (2016).

[9] O. Jitrik, C. F. Bunge, *Phys. Rev. A* **56**, 2614 (1997).

[10] C.X. Almora-Díaz, A. Ramírez-Solís, C.F. Bunge, *Phys. Chem. Chem. Phys.* **21**, 4953 (2019).

[11] C.F. Bunge, *J. Chem. Phys.* **125**, 014107 (2006).

[12] C.F. Bunge R. Carbó-Dorca, *J. Chem. Phys.* **125**, 014108 (2006).

[13] C.D. Sherrill, H.F. Schaefer III, *Adv. Quantum Chem.* **34**, 143 (1999).

[14] E.U. Condon, G.H. Shortley, *The Theory of Atomic spectra*, Cambridge University Press, Cambridge 1964.

[15] C.F. Bunge, J.A. Barrientos, A.V. Bunge, *At. Data Nucl. Data Tables* **53**, 113 (1993).

[16] C. Schwartz, *Phys. Rev.* **126**, 1015 (1962).

[17] C.E. Moore, *Tables of Spectra of Hydrogen, Carbon, Nitrogen and Oxygen Atoms and Ions*, CRC, Boca Raton (FL) 1993.

[18] C.F. Fischer, *Comp. Phys. Comm.* **14**, 145 (1978).

[19] R.E. Brown, Ph.D. Thesis, Indiana University, 1967.

[20] A. Szabo, N.S. Ostlund, *Modern Quantum Chemistry*, Macmillan, New York 1982.

[21] Y. Sun, F. Hu, W.-Y. Li, D.-D. Liu, M.-F. Mei, B.-C. Gou, *Z. Naturforsch.* **76**, 1 (2021).

[22] F. Sasaki, M. Yoshimine, *Phys. Rev. A* **9**, 17 (1974).

[23] P.S. Bagus, A. Hibbert, C. Moser, *J. Phys. B At. Mol. Phys.* **4**, 1611 (1971).

[24] K. Aashaman, T.M. Luke, J.D. Talman, *Phys. Scr.* **27**, 267 (1983).

[25] *CRC Handbook of Chemistry and Physics*, 95th ed., Ed. W.M. Haynes, 2014.